2A.7 EFFECTIVE BUOYANCY AT THE SURFACE AND ALOFT

Nadir Jeevanjee[1,2*], David M. Romps[3,1]

[1]Climate and Ecosystems Science Division, Lawrence Berkeley National Laboratory, Berkeley, CA USA
[2]Department of Physics, University of California at Berkeley, Berkeley, CA USA
[3]Department of Earth and Planetary Sciences, University of California at Berkeley, Berkeley, CA USA

1 Introduction

The Archimedean buoyancy of a fluid parcel is typically offset by the virtual mass effect due to environmental inertia, yielding an 'effective buoyancy' (Davies-Jones, 2003) less than the Archimedean value. Despite its ubiquity, however, this effect is not often quantified and is hard to estimate. In addition to the expected dependence on aspect ratio, recent work (e.g. Jeevanjee and Romps, 2015) also suggests that effective buoyancy depends on surface proximity. We address this by considering idealized buoyant cylindrical parcels of diameter D and height H, deriving analytical expressions for their effective buoyancy both at the surface and aloft.

2 Analytical results

A Poisson equation for the effective buoyancy β was found by Davies-Jones (2003):

$$-\nabla^2(\bar{\rho}\beta) = g\nabla_h^2\rho\ .$$

Here, $\nabla_h^2 \equiv \partial_x^2 + \partial_y^2$ and $\bar{\rho}$ is a reference density profile. Neglecting vertical variations in $\bar{\rho}$ yields an even simpler form in terms of the Archimedean buoyancy $B \equiv -g\frac{\rho'}{\bar{\rho}}$,

$$-\nabla^2\beta = -\nabla_h^2 B\ . \tag{1}$$

*Corresponding author address: Nadir Jeevanjee, UC Berkeley Dept. of Physics, 366 LeConte Hall MC 7300, Berkeley, CA 94720. E-mail: jeevanje@berkeley.edu

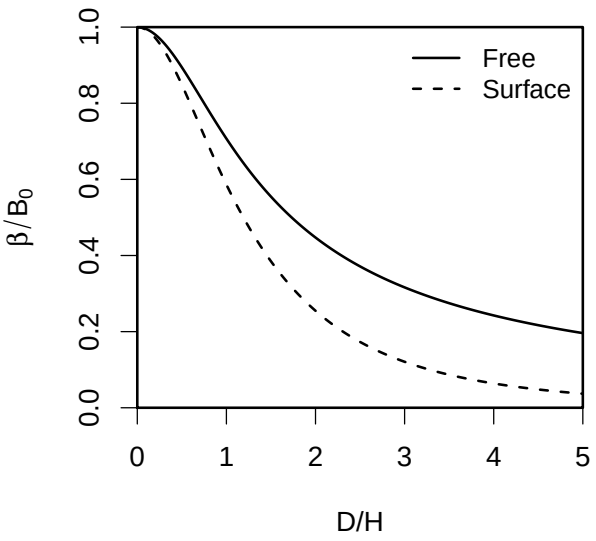

Figure 1: Effective buoyancies at the center of the free cylinder [Eqn. (2), solid line] and the surface cylinder [Eqn. (3), dashed line] as a function of D/H.

We then consider a cylindrical parcel of diameter D, height H, and uniform Archimedan buoyancy B_0. Equation (1) is then amenable to solution via Green's functions, and in particular we find that at the parcel's center,

$$\beta = \frac{B_0}{\sqrt{1 + D^2/H^2}}. \tag{2}$$

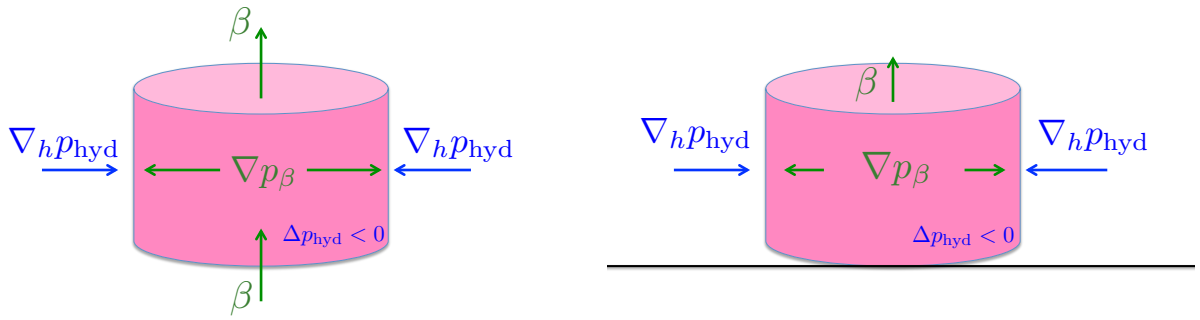

$$|\nabla_h p_\beta| = |\nabla_h p_{\rm hyd}|$$
$$p_\beta = -\Delta p_{\rm hyd}$$

(a) Free cylinder

$$|\nabla_h p_\beta| \neq |\nabla_h p_{\rm hyd}|$$
$$p_\beta < -\Delta p_{\rm hyd}$$

(b) Surface cylinder

Figure 2: Cartoon of the gradients $-\nabla_h p_{\rm hyd}$ and $-\nabla p_\beta$ and associated divergences for **(a)** the free cylinder and **(b)** the surface cylinder. See text for interpretation.

Repeating the analysis for an identical parcel situated at a lower boundary $z = 0$ where $\beta(0) = 0$, we employ the method of images and find

$$\beta = \frac{3B_0}{2}\left(\frac{1}{\sqrt{1 + D^2/H^2}} - \frac{1}{\sqrt{9 + D^2/H^2}}\right) . \quad (3)$$

Both these curves are plotted in Fig. 1. Note that β is is always smaller for the surface cylinder than for the free one, and that it decreases much more rapidly as D/H increases.

3 Intuition

Why does β decline with aspect ratio? And why is this decline so much more marked for surface parcels? To understand this we introduce the *buoyany pressure* p_β, defined by

$$-\nabla^2 p_\beta = \nabla_h^2 p_{\rm hyd} \quad (4)$$

where $p_{\rm hyd}$ is the local (not reference) hydrostatic pressure. Comparison with (1) shows that $\beta = -(\partial_z p_\beta)/\bar{\rho}$. The advantage of considering p_β is that (4) has the simple interpretation that the divergence of $-\nabla p_\beta$ must cancel out any divergence produced by the horizontal hydrostatic pressure gradient $-\nabla_h p_{\rm hyd}$, and β is just the vertical component of $-\nabla p_\beta$.

Cartoons of the p_β field for both the free and surface cylinders are given in Fig. 2. As depicted in panel a, for the free cylinder the $z \to -z$ reflection symmetry of (1) implies that β does not contribute any net divergence into or out of the cylinder, so the convergence from $-\nabla_h p_{\rm hyd}$ must be balanced entirely by horizontal divergence from $-\nabla_h p_\beta$. This relationship can be integrated to yield $p_\beta = -\Delta p_{\rm hyd}$ at cylinder center. For $D \gg H$ p_β stays fixed at $-\Delta p_{\rm hyd}$ but the scale height of p_β varies with D, since that is the dominant length scale of the problem. The effective buoyancy β then scales as

$$\beta \sim \frac{p_\beta}{\bar{\rho} D} \sim -\frac{\Delta p_{\rm hyd}}{\bar{\rho} D} \sim B_0 \frac{H}{D}, \quad (5)$$

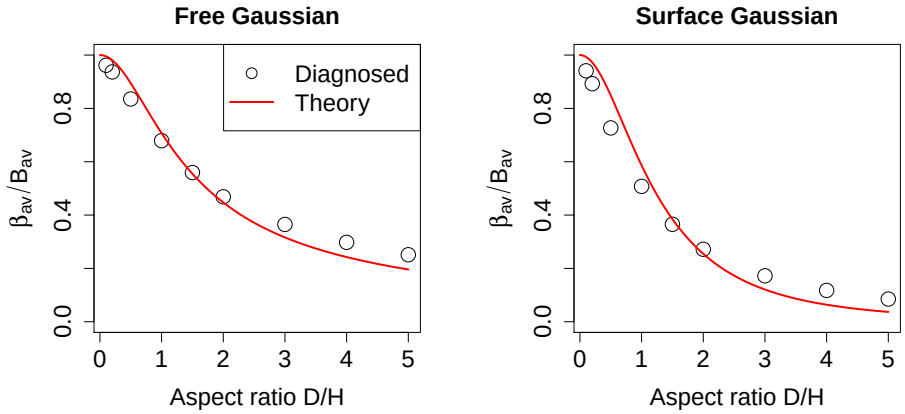

Figure 3: Comparison of the analytical expressions (2) and (3) with numerically diagnosed values of $\beta_{\rm av}/B_{\rm av}$ for Gaussian bubbles with varying D/H.

which is identical to the $D \gg H$ limit of (2).

This explains the decline of β with aspect ratio. What about the effect of the surface? As depicted in Fig. 2b), the $\beta(0) = 0$ boundary condition breaks the $z \to -z$ reflection symmetry and implies that the vertical divergence of β is non-zero. Thus, a smaller value of $|-\nabla_h p_\beta|$ (and its divergence) is sufficient to balance the divergence from $-\nabla_h p_{\rm hyd}$, yielding $p_\beta < -\Delta p_{\rm hyd}$. The smaller value of p_β in turn implies a smaller value of β, and hence it is symmetry breaking by the surface that reduces β for the surface parcel.

4 Applications

Though the formulae (2) and (3) were derived for highly idealized density distributions, one might hope that they would be applicable to more heterogeneous density fields. To test this we construct smooth Gaussian density bubbles of varying aspect ratio and calculate β numerically using a Poisson solver, and then compute the average of both β and B over the bubble. We compare the diagnosed values of $\beta_{\rm av}/B_{\rm av}$ with those predicted by the formulae (2) and (3) in Fig. 3. The agreement is decent, so our formulae, while idealized, do seem to capture something essential about effective buoyancy.

Another application of our formulae would be to understanding the 'grey zone' between hydrostatic and non-hydrostatic regimes in numerical modeling. Interpreting our cylinders as GCM grid cells or columns of horizontal dimension D and height H, the curves in Fig. 1 then provide a quantitative map of the gray zone, telling us how much acceleration to expect from grid-point convection in large-scale or convection-permitting models. For instance, Eqn. (3) tells us that a grid-point surface plume of height 1 km in a convection-permitting model of horizontal resolution 4 km [the threshold identified in the recent review by Prein (2015)] should experience a roughly order-of-magnitude reduction in acceleration from the Archimedean value.

Finally, our results (2) and (3) are essentially just virtual mass coefficients, which are often employed in the vertical velocity equation in convective parameterizations. If aspect ratios for the parcels are estimated, our formulae could be used to diagnose these coefficients and replace the ad-hoc values found in the literature., which currently span a wide range (de Roode et al., 2012).

References

Davies-Jones, R. (2003). An Expression for Effective Buoyancy in Surroundings with Horizontal Density Gradients. *Journal of the Atmospheric Sciences*, 60(23):2922–2925.

de Roode, S. R., Siebesma, a. P., Jonker, H. J. J., and de Voogd, Y. (2012). Parameterization of the Vertical Velocity Equation for Shallow Cumulus Clouds. *Monthly Weather Review*, 140(8):2424–2436.

Jeevanjee, N. and Romps, D. M. (2015). Effective Buoyancy, Inertial Pressure, and the Mechanical Generation of Boundary Layer Mass Flux by Cold Pools. *Journal of the Atmospheric Sciences*, 72(8):3199–3213.

Prein, A. F. (2015). A review on regional convection-permitting climate modeling: Demonstrations, prospects, and challenges. *Reviews of Geophysics*, pages 1–39.